American Mineralogist, Volume 101, pages 1839–1853, 2016

A new EPMA method for fast trace element analysis in simple matrices

John J. Donovan[1,*], Jared W. Singer[2], and John T. Armstrong[3]

[1]CAMCOR, University of Oregon, Eugene, Oregon 97403, U.S.A.
[2]Rensselaer Polytechnic Institute, Troy, New York 12180, U.S.A.
[3]Geophysical Lab, Carnegie Institution for Science, NW Washington, D.C. 20015-1305, U.S.A.

Abstract

It is well known that trace element sensitivity in electron probe microanalysis (EPMA) is limited by intrinsic random variation in the X-ray continuum background and weak signals at low concentrations. The continuum portion of the background is produced by deceleration of the electron beam by the Coulombic field of the specimen atoms. In addition to the continuum, the background also includes interferences from secondary emission lines, "holes" in the continuum from secondary Bragg diffraction, non-linear curvature of the wavelength-dispersive spectrometer (WDS) continuum and other background artifacts. Typically, the background must be characterized with sufficient precision (along with the peak intensity of the emission line of interest, to obtain the net intensity for subsequent quantification), to attain reasonable accuracy for quantification of the elements of interest. Traditionally we characterize these background intensities by measuring on either side of the emission line and interpolate the intensity underneath the peak to obtain the net intensity. Instead, by applying the mean atomic number (MAN) background calibration curve method proposed in this paper for the background intensity correction, such background measurement artifacts are avoided through identification of outliers within a set of standards. We divide the analytical uncertainty of the MAN background calibration between precision errors and accuracy errors. The precision errors of the MAN background calibration are smaller than direct background measurement, if the mean atomic number of the sample matrix is precisely known. For a simple matrix and a suitable blank standard, a high-precision blank correction can offset the accuracy component of the MAN uncertainty. Use of the blank-corrected-MAN background calibration can further improve our measurement precision for trace elements compared to traditional off-peak measurements because the background determination is not limited by continuum X-ray counting statistics. For trace element mapping of a simple matrix, the background variance due to major element heterogeneity is exceedingly small and high-precision two-dimensional background correction is possible.

Keywords: EPMA, quantitative analysis, microanalysis, trace elements, sensitivity, accuracy, X-ray mapping

Introduction

Traditionally electron probe microanalysis (EPMA) has relied upon precise characterization of the continuum intensities adjacent to the emission line of interest for determination of the background under the peak, through interpolation of the off-peak intensities. Recent improvements including new hardware designs with large area Bragg crystals, new software methods implementing exponential and polynomial interpolations to more accurately characterize the curvature of the background, and aggregated spectrometer signals to improve sensitivity, have enabled the EPMA to attain detection limits as low as 2 to 3 ppm in some materials (Donovan et al. 2011).

The traditional off-peak method requires careful selection of background positions to avoid spectral interferences from secondary emission lines near the off-peak intensity positions, and various continuum artifacts (Kato and Suzuki 2014). For trace element characterization, the traditional off-peak method generally requires careful study of a wide swath of the emitted continuum spectrum by means of high-precision WDS scans, which can be quite time consuming. Such spectrometer scanning techniques are particularly time consuming when WDS scans are performed with a precision similar to subsequent trace quantification measurements, to avoid secondary emission lines from other elements when selecting off-peak measurement positions. Unfortunately, even high-sensitivity and time-consuming wavelength scans may not suffice for some samples where the inhomogeneity of major and/or minor elements may introduce unanticipated off-peak interferences on the pre-specified off-peak positions, which may result in significant inaccuracies in the background determination underneath the peak of interest.

Recent work on a new multi-point background method where multiple high-precision off-peak measurements (essentially a sparse high sensitivity wavelength scan combined with typical quantitative peak intensity measurements), for subsequent "iterative" determination of the optimum background positions based on statistical considerations, has been developed for complex matrices where such off-peak interferences are variable in complex materials such

* E-mail: donovan@uoregon.edu

0003-004X/16/0008–1839$05.00/DOI: http://dx.doi.org/10.2138/am-2016-5628

as monazite (Allaz et al., in preparation).

One may also employ time-saving techniques such as only measuring the off-peak intensities every N points, sometimes referred to as Nth point backgrounds, that is unfortunately inadequate for many trace element applications where the matrix composition (and hence background) varies significantly. But in summary, all these trace element techniques require careful interpolation from off-peak intensity measurements to obtain the background intensity under the peak. If only we could directly measure the background intensity under the peak and avoid these interpolation, interference, and other off-peak measurement artifacts entirely.

In fact, it is possible to measure the background directly beneath the peak without interpolation using the MAN background method. This can also be accomplished either using a blank correction by itself (in the case of simple matrices), or even better, using both a blank correction and the MAN background method described in this paper (to deal with differences in composition between the blank standard and the unknown sample). An ideal blank standard has an identical matrix to unknown samples, but is free of trace element contamination. The blank correction is not totally free of spectral artifacts, however the spectral artifacts are similar between unknown and blank.

In this paper, we will demonstrate that, at least for materials with a relatively simple matrix such as SiO_2, TiO_2, or $CaMgSi_2O_6$ or $ZrSiO_4$, where one may obtain suitably well-characterized standards for use in the so called "blank correction," we can obtain comparable trace element accuracy to traditional off-peak methods and improved precision in less time than traditional off-peak methods. The MAN background technique was originally intended to apply only to major and minor element characterization (Donovan and Tingle 1996), but as we will demonstrate, the MAN background method can also be utilized to obtain high-precision trace element characterization without off-peak measurements, by simply measuring the on-peak intensities in several standard materials that do not contain the element of interest. Influence from standard contaminants and/or spectral artifacts can be observed in the MAN regression curve and may be subsequently removed as outliers within the set of MAN standards. Trace element accuracy (typically the MAN background method is limited to around 100 to 200 ppm in most silicates and oxides if the blank correction is not utilized), is assured by use of the "blank correction" technique, so that one may obtain similar accuracy with improved precision, and in approximately half the acquisition time of off-peak trace element measurements. This MAN background method applies not only to point analyses, but also to quantitative X-ray mapping, where the time savings are particularly significant, and improvements in precision are especially noticeable.

Experimental methods

Data for the $CaMgSi_2O_6$ (diopside) off-peak and MAN comparison were acquired on a Cameca SX51 electron microprobe equipped with four tunable wavelength-dispersive spectrometers using Probe for EPMA from Probe Software (probesoftware.com). Operating conditions were 40° takeoff angle, beam energy of 20 keV, beam current of 20 nA, and the beam diameter was 5 μm. Elements were acquired using analyzing crystals LIF for Fe$K\alpha$, Ti$K\alpha$, Mn$K\alpha$, Ni$K\alpha$, K$K\alpha$, and TAP for Na$K\alpha$ and Al$K\alpha$. The standards were TiO_2 synthetic for Ti$K\alpha$, MnO synthetic for Mn$K\alpha$; NiO synthetic for Ni$K\alpha$; labradorite (Lake Co.) for Na$K\alpha$; orthoclase MAD-10 for K$K\alpha$, Al$K\alpha$; and magnetite U.C. no. 3380 for Fe$K\alpha$. The on-peak counting time was 20 s and the off-peak counting time was also 20 s (in total) for all elements. The off-peak correction method was linear interpolation for all elements and the MAN background intensity data was calibrated and continuum absorption corrected for K$K\alpha$, Fe$K\alpha$, Ti$K\alpha$, Na$K\alpha$, Al$K\alpha$, Mn$K\alpha$, Ni$K\alpha$, and all intensities were corrected for dead time. Standard intensities were corrected for standard drift over time and interference corrections were applied to Fe for interference by Mn (Donovan et al. 1993) and a $CaMgSi_2O_6$ matrix was specified by difference. The matrix correction method was $\phi(\rho z)$ and the mass absorption coefficients data set was Henke (LBL 1985). The $\phi(\rho z)$ method algorithm utilized was Armstrong/Love Scott.

Data for the SiO_2 point analyses and quantitative X-ray maps were acquired on a Cameca SX100 electron microprobe equipped with five tunable wavelength-dispersive spectrometers using Probe for EPMA, Probe Image for X-ray map acquisitions and re-processed using CalcImage software also from Probe Software. Operating conditions were 40° takeoff angle, beam energy of 15 keV, beam current was 100 nA, and the beam diameter was 10 μm for the point analysis and 1 μm for the X-ray maps. Elements were acquired using analyzing crystals LLIF for Fe$K\alpha$; LPET for Ti$K\alpha$; PET for K$K\alpha$; and TAP for Al$K\alpha$, Na$K\alpha$. The standards were TiO_2 synthetic for Ti$K\alpha$; nepheline for Na$K\alpha$; and orthoclase MAD-10 for K$K\alpha$, Al$K\alpha$; and magnetite U.C. no. 3380 for Fe$K\alpha$. The off-peak correction method was linear interpolation for Fe$K\alpha$, K$K\alpha$, Na$K\alpha$, average for Al$K\alpha$, and exponential for TiK (generally one should use a polynomial or exponential interpolation for Al$K\alpha$ in SiO_2 because the Al$K\alpha$ peak is on the tail of the Si$K\alpha$ line, but the blank correction deals with this issue effectively, so the fit method is a moot point in this case). Unknown and standard intensities were corrected for dead time. Oxygen was calculated by cation stoichiometry and included in the matrix correction. Si was calculated by difference from 100%. The matrix correction method was $\phi(\rho z)$ by Armstrong/Love Scott. The SiO_2 blank by laser ablation ICP-MS gave 1.4 ppm Ti and AA gave 15 ppm Al and 6 ppm Fe.

Data for the $ZrSiO_4$ point analyses were obtained using a synthetic zircon from John Hanchar (Memorial University), and quantitative X-ray maps using SIMS Oxygen standard AS3, all acquired on a Cameca SX100 electron microprobe equipped with five tunable wavelength-dispersive spectrometers using Probe for EPMA for the standard intensities, Probe Image for X-ray map acquisition and re-processed using CalcImage software also from Probe Software. Operating conditions were 40° takeoff angle, beam energy of 20 keV, beam current was 100 nA, and the beam diameter was 5 μm for the point analyses and 1 μm for the X-ray map acquisitions. Elements were acquired using analyzing crystals PET for Th$M\alpha$, Y$L\alpha$; LPET for U$M\alpha$, P$K\alpha$; PET for Th$M\alpha$, Y$L\alpha$; and TAP for Hf$M\alpha$. The standards were UO_2 for U$M\alpha$; $ThSiO_4$ (thorite) for Th$M\alpha$; $HfSiO_4$ (hafnon) for Hf$M\alpha$; and YPO_4 (USNM 168499) for P$K\alpha$ and Y$L\alpha$. The on-peak and off-peak counting time for point analyses was 640 s for all elements. The off-peak correction method was linear for Th$M\alpha$, U$M\alpha$, Y$L\alpha$, and exponential for P$K\alpha$ and Hf$M\alpha$. Unknown and standard intensities were corrected for dead time. Standard intensities were corrected for standard drift over time. Point analysis results are the average of 5 points. Si, Zr, and O were specified for the matrix correction. The quantitative blank correction was utilized based on a synthetic zircon from Lynn Boatner (Oak Ridge National Laboratory), which was characterized by laser ablation ICP-MS measurements by Alan Koenig (USGS Denver) and yielded 15 ppm Hf, 25 ppm Y, and below detection limit (<1 ppm) for U and Th. Phosphorus was not characterized due to difficulties with the LA-ICP-MS method for this element. The matrix correction method was the $\phi(\rho z)$ algorithm by Armstrong/Love Scott.

MAN background corrections

An alternative background correction method known as the mean atomic number (MAN) background correction, based on Kramer's Law (Kramers 1923)

$$N(E) = iZ\left[\left(E_O - E\right)/E\right]dE$$

has been in use for over 20 years now. Although originally designed for EPMA monochromators that cannot be "detuned" off-peak, the method has been extended and improved for all types of Bragg spectrometers by the use of multiple standards and linear or polynomial regression of the measured on-peak intensities in standards that do not contain the element of interest.

Further improvement has been accomplished by correction for continuum absorption (Armstrong 1988), based on a modified form of the relationship between $\overline{Z}$ and intensity by Ware and Reed that includes a correction for continuum absorption by the specimen (Ware and Reed 1973) where I(E) is the background intensity as a function of i, Z, E_O, E, and $f(x)$, where i is the beam current, Z is the average atomic number, E_O is the beam energy, E is the energy of the emission and $f(x)$ is the matrix correction all integrated over the energy range:

$$\mathrm{I(E)} = \mathrm{iZ}\left\{\left[\frac{\left(E_O - E\right)}{E}\right] f(x)\right\} dE$$

The continuum absorption correction improves accuracy and regression precision, since each standard material utilized in the MAN regression curve will have different absorption effects on the particular (on-peak) photon energy of interest.

MAN BACKGROUND METHOD ITERATION

It should be noted that because the MAN background intensities are recalculated during each iteration of the matrix correction, we require two iteration loops in our quantification method. One loop for the normal matrix correction (whatever physics algorithm that might be), and a second outer iteration loop for all the compositionally dependent corrections such as: MAN backgrounds, quantitative spectral interferences, and compound area-peak factors for chemical shifts and peak shape changes.

This double iteration loop allows the program to "refine" the calculated MAN background as the composition of the unknown converges (MAN background correction of standard intensities is trivial since their compositions are already known and hence their average Z is fixed). For unknowns the process is performed in several steps. First, the on-peak intensities for several standards not containing the element of interest and covering a range of atomic numbers for the standards and anticipated unknown compositions are acquired by the analyst (or reloaded from a previous MAN calibration). Second, the on-peak intensities on the standards used for the MAN calibration are corrected for continuum absorption by the simple relation:

$$I_{COR} = I_{RAW} \cdot \mathrm{ZAF}^S$$

where I_{COR} is the absorption corrected intensity for the MAN standard, and ZAF^S is the absorption correction for the standard composition (note that the ZAF^S term here is the inverse of the $f(x)$ term in Ware and Reed's expression). This "virtual" intensity MAN calibration curve, which has been corrected for continuum absorption, is then stored for subsequent use for MAN background correction of unknown compositions. During the iterated matrix correction of the unknown intensities, we initially assume an arbitrary $\overline{Z}$ for the unknown, and then calculate the background intensity from our previously acquired and stored "virtual" MAN intensity regression. This calculated average Z is then improved as the composition converges during the matrix iteration. Finally we de-correct the calculated background intensity for the continuum absorption associated with the actual unknown composition as seen here:

$$I_{RAW} = I_{COR}/\mathrm{ZAF}^U$$

where ZAF^U is the absorption term for the unknown composition undergoing iteration. The I_{RAW} background intensity is then simply subtracted from the measured unknown on-peak intensity to obtain the background corrected intensity for the unknown composition. This calculation proceeds until the composition (and hence average Z) converges, and a proper background correction has been applied.

The measured standard intensities should be corrected for continuum absorption to improve regression accuracy and precision, especially at sub 100 to 200 ppm levels. As mentioned above, a continuum absorption "de-correction" must also be applied to the regressed MAN background intensity due to the fact that the unknown specimen intensity will generally have a different specimen matrix than the standards utilized for the MAN calibration curve. The effect of the continuum absorption is most significant for low-energy emission lines from elements such as sodium, magnesium, etc., as seen in Figures 1 and 2. For higher-energy emission lines from such elements as potassium and iron, the continuum absorption correction effect is decreased, but still significant for best accuracy as seen in Figures 3 and 4. Note that because the differences in continuum absorption primarily contributes toward a larger variance as opposed to an absolute change in the intensity regression fit, the absence of a continuum absorption correction is a minor effect except in cases of low-energy emission lines such as Na$K\alpha$, Mg$K\alpha$, etc.

PRECISION OF MAN BACKGROUND METHOD

The MAN background method is capable of higher precision than traditional off-peak background determinations particularly when the measured matrix $\overline{Z}$ variance from the major elements is small. That is, the MAN $\overline{Z}$ variance for trace element analysis is typically small because it is based on either measurements of high intensity X-rays from the major elements or matrix specification by difference or fixed concentration elements. Also the MAN background method can achieve a low correlation variance if suitably known and pure reference materials are used and the above continuum absorption correction is appropriately applied. In contrast, off-peak background intensities are relatively weak signals with associated poor counting statistics, therefore interpolation from off-peak intensity measurements imbues an intrinsically larger variance.

To highlight the improved precision of the MAN background method, we compare the propagated net intensity variance for off-peak and for MAN background correction methods derived from the generalized variance equation for function f of i principal variables: The total variance of a function or an operation (f) is the square root of the summation of all partial differential equations multiplied by each constituent variance, for i principal variables as seen here:

$$\sigma_f(i) = \sqrt{\sum_i \left(\frac{\partial f}{\partial i}\sigma_i\right)^2}\ .$$

For any method of background correction (off-peak, MAN, or Nth point), the background intensity (B) is subtracted from the peak intensity (P) for the net intensity (I_{net}):

$$I_{net}(P,B) = P - B.$$

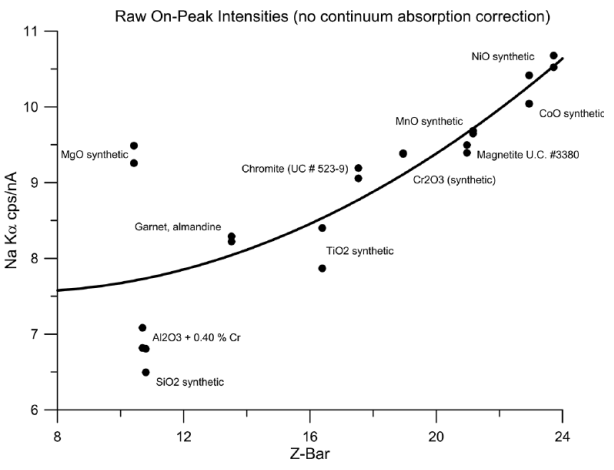

Figure 1. MAN (on-peak) background calibration curve for Na*K*α, (20 keV, 20 nA, 5 μm, 20 s integration time using TAP crystal) uncorrected for continuum absorption. Second-order polynomial fit yields an average relative deviation of ~8.5%.

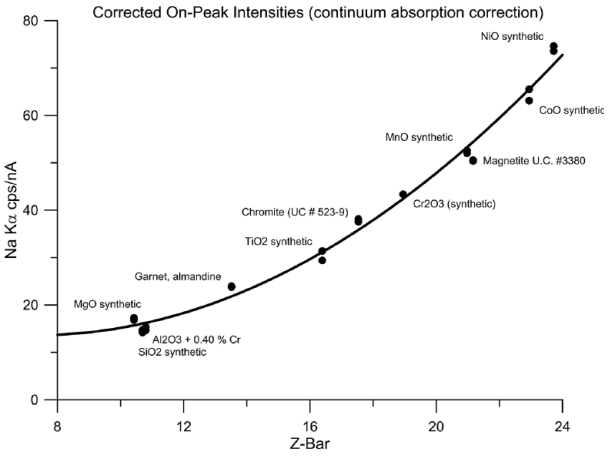

Figure 2. MAN (on-peak) background calibration curve for Na*K*α, (20 keV, 20 nA, 5 μm, 20 s integration time using TAP crystal) corrected for continuum absorption. Second-order polynomial fit yields an average relative deviation of ~5.5%.

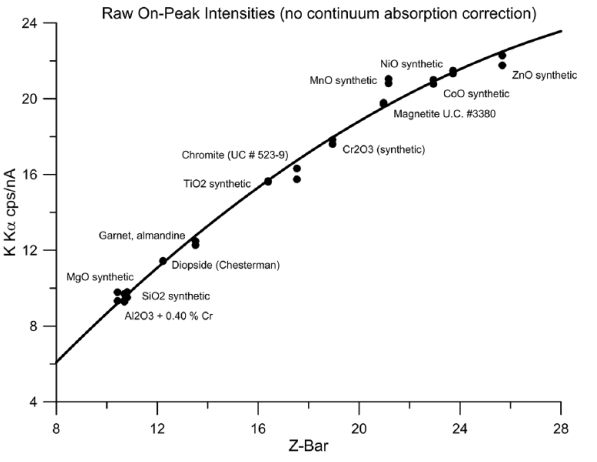

Figure 3. MAN (on-peak) background calibration curve for K*K*α, (20 keV, 20 nA, 5 μm, 20 s integration time using PET crystal) uncorrected for continuum absorption. Second-order polynomial fit yields an average relative deviation of ~2.6%.

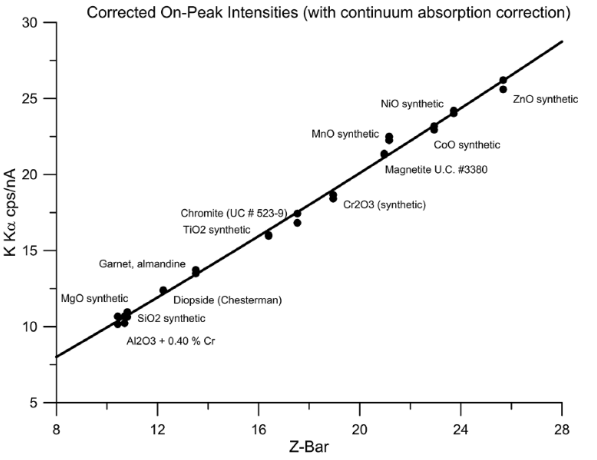

Figure 4. MAN (on-peak) background calibration curve for K*K*α, (20 keV, 20 nA, 5 μm, 20 s integration time using PET crystal) corrected for continuum absorption. Second-order polynomial fit yields an average relative deviation of ~2.1%.

The partial derivatives in the case of subtraction are negligible, and the variance equation becomes

$$\sigma_{\text{net}} = \sqrt{\left(1 \cdot \sigma_P\right)^2 + \left(-1 \cdot \sigma_B\right)^2}$$

and we simplify to the familiar expression for net intensity variance

$$\sigma_{\text{net}} = \sqrt{\sigma_P^2 + \sigma_B^2}\,.$$

Traditionally the peak and background variance is determined directly from counting statistics, and for a single measurement this error estimate does not include other sources of variance such as standard homogeneity, spectrometer movement, beam current measurement, environmental stability, and so on. For linear off-peak background interpolation (B_{OFF}), the interpolation in slope-intercept form is $B_{OFF}(x,m,b) = m \cdot x + b$.

There are three principal variables, namely x spectrometer coordinate, m background slope, and b the interpolation intercept. The propagated off-peak background variance ($\sigma_{B,\,OFF}$) is

$$\sigma_{B_{OFF}} = \sqrt{\left(\frac{\partial B_{OFF}}{\partial x}\sigma_x\right)^2 + \left(\frac{\partial B_{OFF}}{\partial m}\sigma_m\right)^2 + \left(\frac{\partial B_{OFF}}{\partial b}\sigma_b\right)^2}\,.$$

The partial derivatives of B_{OFF} are

$$\frac{\partial B_{OFF}}{\partial x} = m \qquad \frac{\partial B_{OFF}}{\partial m} = x \qquad \frac{\partial B_{OFF}}{\partial b} = 1.$$

The off-peak background variance (σ_B) simplifies to the following

$$\sigma_{B_{OFF}} = \sqrt{\left(m \cdot \sigma_x\right)^2 + (x \cdot \sigma_m)^2 + (1 \cdot \sigma_b)^2}\,.$$

The propagated off-peak background variance is commonly ignored, because two-point interpolation allows no estimates of slope and intercept variance (σ_m and σ_b). However in the case of replicate measurements using off-peak background corrections, each of the above terms arise naturally from the measurement process. The first term ($m \cdot \sigma_x$) indicates that spectrometer reproducibility (σ_x) is exacerbated when the background is increasingly sloped. The correlation variance, terms $(x \cdot \sigma_m)^2$ and $(\sigma_b)^2$, aggregate many sources of variance that would affect the quality of the linear regression including systematic error when the true background is not linear. When the propagated off-peak background variance is neglected (along with factors affecting the on-peak variance), the error estimates for a single analysis will be arbitrarily small compared to the real fluctuations of replicate measurements. If off-peak correlation variance were possible to estimate (such as for multi-point, off-peak), the weak background intensities may lead to large correlation variance without significant time investment in background characterization.

The propagated MAN background variance ($\sigma_{B,MAN}$) is derived from a background intensity correlation function (B_{MAN}), which may be specified according to the operator of best fit, including linear or second-order polynomial. For Kramer's Law the expected dependence of background intensity on $\overline{Z}$ is linear, however curvature well fit by a second-order polynomial is often observed. For the linear case, the MAN background intensity is correlated with $\overline{Z}$ (the average atomic number) in the form of a line with slope (m) and intercept (b):

$$B_{MAN}\left(\overline{Z},\, m,\, b\right) = m \cdot \overline{Z} + b\,.$$

Thus the MAN background variance is,

$$\sigma_{B_{MAN}} = \sqrt{\left(\frac{\partial f}{\partial \overline{Z}}\sigma_{\overline{Z}}\right)^2 + \left(\frac{\partial f}{\partial m}\sigma_m\right)^2 + \left(\frac{\partial f}{\partial b}\sigma_b\right)^2}\,.$$

For the linear case the partial derivatives are

$$\frac{\partial B_{MAN}}{\partial \overline{Z}} = m \qquad \frac{\partial B_{MAN}}{\partial m} = \overline{Z} \qquad \frac{\partial B_{MAN}}{\partial b} = 1\,.$$

Combining these terms we arrive at an intermediate result

$$\sigma_{B_{MAN}} = \sqrt{\left(m \cdot \sigma_{\overline{Z}}\right)^2 + \left(\overline{Z} \cdot \sigma_m\right)^2 + \left(1 \cdot \sigma_b\right)^2}$$

which emphasizes the basic dependencies of the MAN background variance on $\overline{Z}$ and correlation variance. For example, as $\overline{Z}$ becomes large, the MAN background variance depends more strongly on the slope variance (σ_m); likewise as the slope becomes large, the MAN background variance depends strongly on $\overline{Z}$ variance ($\sigma_{\overline{Z}}$). The slope and intercept variances are calculated from the residuals of the best-fit (not derived here) and practically the MAN correlation variances depend on factors including the purity of the standards used to generate the MAN background correlation, on the absence of on-peak interferences, and on application of the absorption correction (discussed in the previous section). As for off-peak methods, the propagated correlation variance may aggregate numerous sources of error (both random and systematic).

The $\overline{Z}$ value is obtained from concentration weighted averaging, since we are estimating the average strength of the Coulombic field of the atoms composing the specimen matrix (Donovan and Pingitore 2002), which is in turn of course determined by the number of electrons in the specimen matrix atoms. And since A/Z is approximately a constant over the periodic table it provides a reasonable weighting for average atomic number in compounds. Hence the mean atomic number ($\overline{Z}$) is calculated from the summation of the atomic numbers multiplied by the weighted fractions (c_i) for all elements i in the total composition:

$$\overline{Z} = \sum_i c_i \cdot Z_i\,.$$

The sum of the concentration weighted fractions must sum close to one to ensure the completeness of the matrix $\overline{Z}$ calculation. The partial derivatives of the $\overline{Z}$ operator are

$$\frac{\partial \overline{Z}}{\partial c_i} = Z_i \qquad \frac{\partial \overline{Z}}{\partial Z_i} = c_i\,.$$

It follows that the $\overline{Z}$ variance is a series for $i = 1$ to $i = n$ elements in the total composition:

$$\sigma_{\overline{Z}} = \sqrt{\left(\frac{\partial \overline{Z}}{\partial c_1}\sigma_{C_1}\right)^2 + \left(\frac{\partial \overline{Z}}{\partial Z_1}\sigma_{Z_1}\right)^2 + \ldots\left(\frac{\partial \overline{Z}}{\partial c_n}\sigma_{C_n}\right)^2 + \left(\frac{\partial \overline{Z}}{\partial Z_n}\sigma_{Z_n}\right)^2}\,.$$

Substituting the simplified partial derivatives we obtain

$$\sigma_{\overline{Z}} = \sqrt{\left(Z_1 \cdot \sigma_{C_1}\right)^2 + \left(c_1 \cdot \sigma_{Z_1}\right)^2 + \ldots\left(Z_n \cdot \sigma_{C_n}\right)^2 + \left(c_n \cdot \sigma_{Z_n}\right)^2}\,.$$

An individual atomic number Z_i is a physical constant (therefore, $\sigma_{Zi} = 0$), and ($c_i \cdot \sigma_{Zi}$) terms drop out:

$$\sigma_{\overline{Z}} = \sqrt{\left(Z_1 \cdot \sigma_{C_1}\right)^2 + \ldots\left(Z_n \cdot \sigma_{C_n}\right)^2}$$

$$\sigma_{\overline{Z}} = \sqrt{\left(\sum_i Z_i \cdot \sigma_{C_i}\right)}\,.$$

The above equation shows that elements having large atomic numbers have a disproportionate effect on the $\overline{Z}$ variance. However, it is important to note that regardless of the absolute value of Z_i, major elements will contribute the largest portion of the concentration-weighted variance. Individual concentration weighted variances (σ_{ci}) for elements i to n are obtained by direct analysis or in the case of a simple sample matrix, the major element concentration (c_{major}) and major element variances may be inferred by difference from i trace element concentrations:

$$c_{major} = 1 - \sum_i c_i\,.$$

The average Z variance of measured matrix elements (those elements not by fixed concentration or specified by difference) is the following expression:

$$\sigma_{C_{\text{major}}} = \sqrt{\left(\sum_i \sigma_{C_i}^2\right)}.$$

Bringing the various statements together, the propagated MAN background variance in the case of linear correlation is

$$\sigma_{B\ MAN} = \sqrt{\left(m \cdot \sqrt{\sum_i \left(Z_i \sigma_{C_i}\right)^2}\right)^2 + \left(\bar{Z} \cdot \sigma_m\right)^2 + \left(1 \cdot \sigma_b\right)^2}.$$

This full propagated error expression with the MAN correlation variance terms will be referred to as "Model A" in the discussion. Now if the MAN correlation variance is considered an accuracy issue (see discussion in the Accuracy vs. Precision in the MAN Background Method section for further explanation), the variance on the MAN background intensity simplifies to this expression that only includes the variance in the specimen matrix average Z and the slope of the MAN regression:

$$\sigma_{B\ MAN} = m \cdot \sqrt{\sum_i \left(Z_i \sigma_{c_i}\right)^2}.$$

Note that the above expression, without the MAN regression precision terms, is referred to as "Model B" in subsequent discussion.

Before we proceed, it may be instructive to consider the time savings and precision increase in the case of so-called Nth point off-peak backgrounds where the analyst measures the off-peak background only every N acquisitions where N is greater than 1. The idea being that subsequent acquisitions only measure the on-peak intensities and simply re-utilize the initial off-peak measurement. In this case, the background intensity is treated as a constant (for those replicate measurements) and hence the background intensity variance on these subsequent measurements is zero. The tradeoff is that the background intensity accuracy of these subsequent analyses is unknown since the background is no longer being measured directly. Thus, the Nth point background correction is only suitable for highly homogeneous materials. The time savings (approaching half) may be achieved if the background is measured only once by the Nth point background correction for a set of on-peak analyses. Increase in precision can be rationalized practically, because spectrometer movement can be minimized and time-dependent sources of variance may also be mitigated through time savings. Mathematically, we are subtracting a constant background value for replicate peak measurements; therefore when using an Nth point background method, the observed replicate net intensity variance includes only the on-peak variance.

In a similar manner the MAN method does not directly measure the background intensity for every measurement, but instead calculates the background for the unknown in question based on the measured composition (average atomic number) of the unknown data point (unlike the Nth point background method, the MAN background method automatically handles changes in matrix composition), and the previously acquired MAN calibration curve, which is based on on-peak intensity measurements on standards that do not contain the element(s) of interest. In other words, a single MAN calibration curve is utilized for many replicate measurements, and since for a given average Z, the same background intensity will be obtained, the variance of replicate calculations is not precisely zero, but instead very close to zero. In general, we can improve our sensitivity by approximately the square root of 2 when $P \approx B$ because the MAN background variance term approaches zero in the case of a fixed matrix and is only slightly larger in the case of a measured matrix, because the MAN background determination is dominated by the major element intensities. At the same time we reduce our total X-ray integration time by some 50% because we are only measuring the on-peak intensities for our trace elements.

Use of the blank correction to improve accuracy for trace MAN analyses

Although we are able to improve precision and reduce acquisition time by means of the MAN background correction, we must still deal with the issue of accuracy at the trace level since there will always be systematic artifacts at some trace level in the X-ray continuum spectrum. To improve accuracy of our MAN background modeling, due to the possible imperfect nature of the reference materials and the continuum modeling used in the MAN regression, the "blank" correction can be applied for further improvement in trace element accuracy in specimens (SiO_2, TiO_2, $ZrSiO_4$, etc.) when a blank [or non-zero concentration] secondary standard with a matching matrix is available. A true blank (zero; below detection limit) is more preferred than low-level reference materials; if a non-zero concentration reference material is used, then the overall accuracy of EPMA is predicated on the systematic errors of another technique. Fortunately for specimens with simple matrices such as SiO_2, TiO_2, $CaMgSi_2O_6$, $ZrSiO_4$, etc., we can easily improve MAN background accuracy by use of the "blank" correction method previously described. Although originally intended for off-peak measurements, where secondary Bragg reflection and sample absorption edges can produce artifacts as large as 50 ppm, the blank correction allows the MAN background correction to achieve accuracy similar to the precision with which the blank standard was measured.

As discussed, the MAN method is based on measuring the on-peak intensities for several standards, which do not contain an element of interest, but also cover the range of average atomic number ($\bar{Z}$) for the unknowns and standards being utilized. The typical $\bar{Z}$ range for oxides and silicates is generally from 10 to 20 and therefore simple oxides such as MgO, Al_2O_3, SiO_2, TiO_2, and MnO or NiO are usually ideal for such purposes. Therefore, these MAN calibration standards can be any material with appropriate $\bar{Z}$ values that do not contain the element of interest (on-peak interferences can be avoided with a simple review of the regression fit since interferences or unsuspected contamination for that matter will always show as outliers above the general curve of the regression).

The accuracy of the MAN background correction can be ascertained by acquiring the complete on- and off-peak intensities and calculating the background correction using both off-peak and MAN methods on the same data set, since the MAN background correction simply ignores the off-peak data, if it was acquired. A comparison between off-peak and MAN methods performed on a $CaMgSi_2O_6$ (diopside) standard candidate is shown in Table 1, where it can be seen that the concentration

differences between the off-peak and MAN methods are less than the reported variance of the measurements. For example, off-peak measurements of Na yield 160 ppm Na and –10 ppm K, but, using the MAN background corrections on the same intensity data, we obtain essentially the same concentration results (170 ppm Na and 10 ppm K) that are within the precision of the measurements.

A further comparison of synthetic SiO_2 is seen in Tables 2a and 2b where again the off-peak and MAN background corrections produce results that are within 100 ppm of each other. Table 2c shows the results for the MAN analyses where the blank correction has been applied from our SiO_2 standard, and it can be seen that the accuracy is now equal to or better than the measured variance when compared to ICP-MS analyses.

For a further test, we acquired both traditional off-peak and the MAN background corrected point intensities for Ti and Al in a natural quartz (Audetat) in separate acquisitions. Results acquired using both off-peak background and MAN background methods are shown for Ti in Figure 5 and for Al in Figure 6. Note that these point analyses were acquired separately as both off-peak and MAN acquisitions, separated in time (proxy to line numbers). Of course this accuracy improvement generally only pertains to specimen matrices with relatively simple compositions for which a suitable "blank" standard containing a zero (or known non-zero) concentration is available. But this may include pure metals, pure oxides, simple silicates and sulfides, etc., so a large number of materials can benefit from this trace element method.

TABLE 1. $CaMgSi_2O_6$ (diopside) standard analyzed for traces as an "unknown" using traditional off-peak intensity background corrections, compared to MAN background corrections (20 keV, 20 nA, 5 µm beam, 20 s on-peak integration time, 20 s off-peak integration time, average of 10 points)

Element	X-ray	Crystal	Off-peak wt%	St.dev.	MAN wt%
K	*Kα*	PET	–0.001	0.004	0.001
Fe	*Kα*	LIF	0.05	0.015	0.051
Ti	*Kα*	LIF	–0.001	0.008	0.003
Na	*Kα*	TAP	0.016	0.009	0.017
Al	*Kα*	TAP	0.026	0.006	0.014
Mn	*Kα*	LIF	0.007	0.008	–0.005
Ni	*Kα*	LIF	0.002	0.009	–0.003

Note: The differences in the concentrations between off-peak and MAN are within the measured variances.

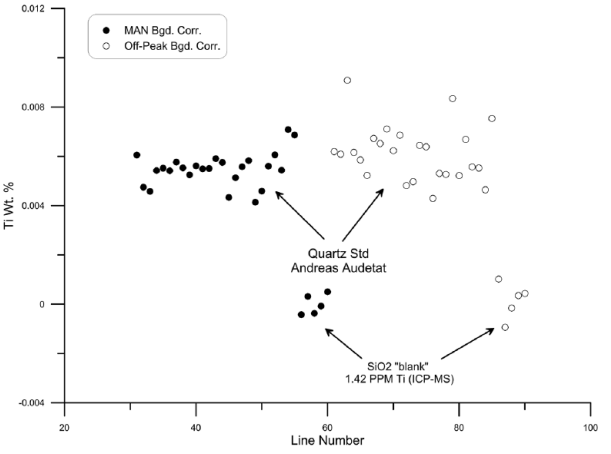

FIGURE 5. Ti wt% in Audetat natural quartz standard. MAN vs. off-peak, Ti*K*α (LIF/LLIF), 20 keV, 100 nA, 10 µm, 200 s on-peak (200 s off-peak), Both data sets are aggregates from two spectrometers and blank corrected. "Line number" refers to the acquisition order.

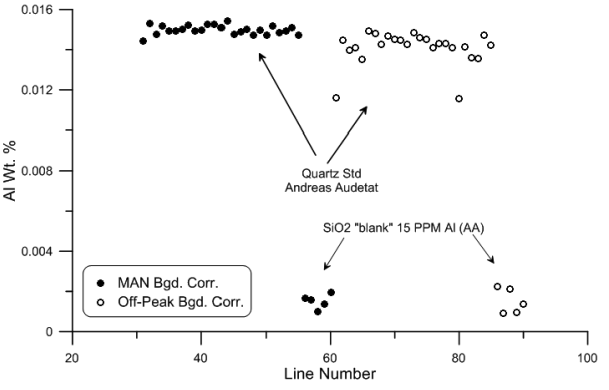

FIGURE 6. Al wt% in Audetat natural quartz standard. MAN vs. off-peak, Al*K*α (TAP/LTAP), 20 keV, 100 nA, 10 µm, 200 s on-peak (200 s off-peak). Both data sets are aggregates from two spectrometers and blank corrected. The line numbers are proxy for acquisition order and show alternating acquisitions between off-peak and MAN measurements. Outliers on off-peak measurements may represent spectrometer reproducibility problems that are not seen with MAN measurements.

TABLE 2a. Off-peak analysis of synthetic SiO_2, 15 keV, 100 nA, 10 µm beam, 180 s on-peak, and 180 s off-peak; average of 5 points; without the blank correction applied

	Ti	Fe	Al	K	Na	Si	O	Total
Average	–0.00095	0.00154	0.00294	0.00018	0.00021	46.740	53.256	100.000
St.dev.	0.00105	0.00139	0.00097	0.00092	0.00108	0.001	0.00060	0.000
%Rel St.dev.	–116.10	89.75	32.95	523.27	525.57	–	–	–

TABLE 2b. MAN analysis of standard SiO_2, 15 keV, 100 nA, 10 µm beam, 180 s on-peak; average of 5 points; without the blank correction applied

	Ti	Fe	Al	K	Na	Si	O	Total
Average	–0.00300	–0.00487	0.00438	–0.00128	–0.00402	46.748	53.261	100.000
St.dev.	0.00034	0.00146	0.00053	0.00042	0.00062	0.001	0.00046	0.000
%Rel St.dev.	–11.43	–29.99	12.09	–32.99	–15.52	–	–	–

Note: Significantly improved standard deviations in the results for the MAN background correction compared to the traditional off-peak method seen in Table 2a.

TABLE 2c. MAN analysis of standard SiO_2, 15 keV, 100 nA, 10 µm beam, 180 s on-peak; average of 5 points; with the blank correction applied from the SiO_2 bulk standard to itself, the accuracy now is similar to the precision of the measurements

	Ti	Fe	Al	K	Na	Si	O	Total
Average	0.00013	0.00059	0.00150	–0.00001	0.00052	46.741	53.2564	100.000
St.dev.	0.00034	0.00146	0.00053	0.00042	0.00063	0.001	0.00046	0.000

Notes: ICP-MS = Ti 1.42 ppm. AA = Fe 6 ± 3 ppm, Al 15 ± 5 ppm, Na 5 ± 3 ppm.

X-ray mapping and MAN background corrections

Although the use of the MAN background correction method combined with the blank correction for trace element point analyses results in acquisition times that are approximately half that of normal off-peak measurements (while improving precision and maintaining accuracy similar to the precision of the on-peak intensity), similar time savings results from the use of the MAN background correction for X-ray mapping. This is because one need only acquire the on-peak intensity map, since the background is calculated based on the MAN fit to point acquisitions of standards not containing the element of interest as described above.

Mapping results (based three X-ray map acquisitions for each sample: the on-peak intensity pixel map, the high side pixel intensity map, and the low side pixel intensity map—note that MAN results utilize only the on-peak intensity map) are shown for pure synthetic SiO_2, first with off-peak map pixel intensities interpolated and subtracted from the on-peak pixel intensities in Figure 7a, using the same raw intensity acquisition data set on the SiO_2 sample for both background correction methods (with the on-peak pixel intensities corrected using the MAN calibration curve from standards applied in Fig. 7b). Note the significant improvement of the MAN background intensity precision. In fact the variance of the MAN background intensities is due only to the variance of the trace elements effect on the average Z calculation. Again, if we consider Nth point statistics, the background variance for Nth point intensities is zero because the background intensity is constant, but accuracy suffers since the Nth point background method does not account for changes in composition as the MAN method does automatically.

It should be noted that typical X-ray mapping integration times per pixel of a few seconds or less are generally of insufficient sensitivity to warrant the use of the blank correction in silicates and oxides, although it can be applied if a suitable blank standard can be obtained for the material in question if necessary. In other words, only when the per pixel X-ray mapping sensitivity begins to approach typical MAN accuracy of around 100 to 200 ppm (in silicates and oxides) is the blank correction step actually necessary for X-ray mapping.

In the case of the SiO_2 background intensity maps shown in Figure 7b, one can see that the MAN background intensity variances are several orders of magnitude smaller than a direct measurement of the backgrounds using the off-peak method in Figure 7a. In fact the measured concentrations shown in Figures 8a and 8b are well below the detection limit of approximately 100 ppm as shown in the detection limit maps for the same SiO_2 specimen for all elements measured in Figures 9a and 9b. It is evident that the calculated pixel detection limits for off-peak measurements shown in Figure 9a has a greater variation compared to the pixel detection limits for MAN measurements due to the variance as seen in the interpolated off-peak intensity maps (Fig. 7a). On the other hand, the MAN detection limit maps show more constant detection limits, which is as expected due to the MAN background being essentially a constant for the given average atomic number (composition of SiO_2 gives ~10.4 $\bar{Z}$).

Application to amethyst and zircon

Figures 9c and 9d compare traditional off-peak X-ray maps for synthetic SiO_2 with the same measured intensity data processed using MAN background and utilizing only the on-peak

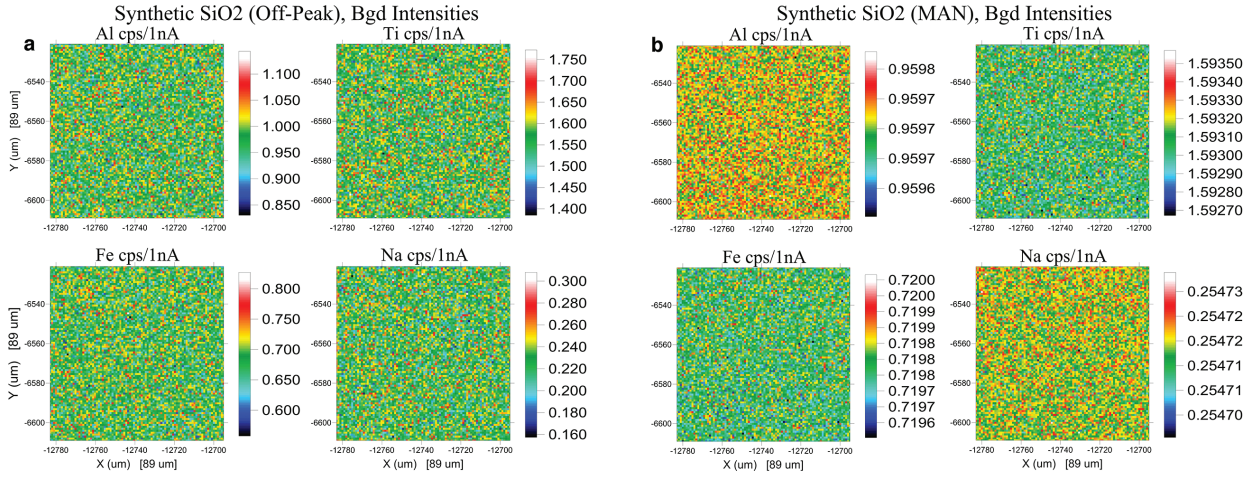

Figure 7. (**a**) Calculated background intensities using a linear interpolation of the measured off-peak pixel intensities using high side and low side off-peak positions for Al$K\alpha$, Ti$K\alpha$, Fe$K\alpha$, and Na$K\alpha$ in synthetic SiO_2, 15 keV, 100 nA, 6000 ms on-peak, 3000 ms off-peak (×2). Note that the calculated background intensities show the expected variance from the off-peak measurement uncertainties. (**b**) Calculated background intensities using a linear regression curve from the measured on-peak pixel intensities for several standard materials that do not contain the elements of interest. Al$K\alpha$, Ti$K\alpha$, Fe$K\alpha$, and Na$K\alpha$ in synthetic SiO_2, 15 keV, 100 nA, 6000 ms on-peak. Note that the calculated background intensities show a much smaller degree of variance. This is due to the fact that the MAN calibration curve always returns the same intensity value for a given average Z, which is based on the measured composition. Since the composition is this case (pure SiO_2) is essentially constant (the variation in the trace elements causes some small degree of calculated average Z), the calculated is also essentially a constant. The fact that a re-measurement of the MAN regression curve will produce slightly different (but again essentially constant intensities for a given average Z) indicates an accuracy error that must be corrected using the blank correction step as described in the text.

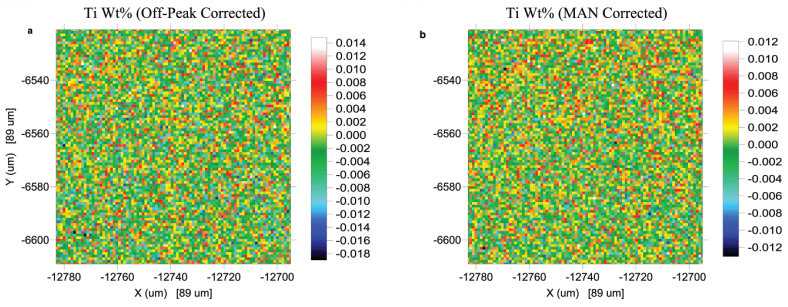

Figure 8. (**a**) Ti wt% in synthetic SiO_2, 15 keV, 100 nA, 6000 ms on-peak, 3000 ms off-peak (×2) and processed using measured off-peak backgrounds. (**b**) Ti wt% in synthetic SiO_2, 15 keV, 100 nA, 6000 ms on-peak (only) and processed using measured MAN standard calibration curve in half the acquisition time (using the on-peak intensities from **a**). The average (zero) difference between the two maps is approximately 20–30 ppm, without any "blank correction."

intensities. This results in improved precision in approximately half the acquisition time (assuming trace acquisitions where the on- and off-peak pixel integration times are roughly equal).

The improvement in trace sensitivity shown above for SiO_2 and amethyst are significant, but with an average Z of roughly 10, the continuum intensities are relatively low and the peak to background ratios quite good.

However, for the case of zircon ($ZrSiO_4$), with an average atomic number of approximately 24, we can expect a larger correction for background intensity. Again we acquired point analyses and X-ray maps on two synthetic zircons and a natural zircon (SIMS

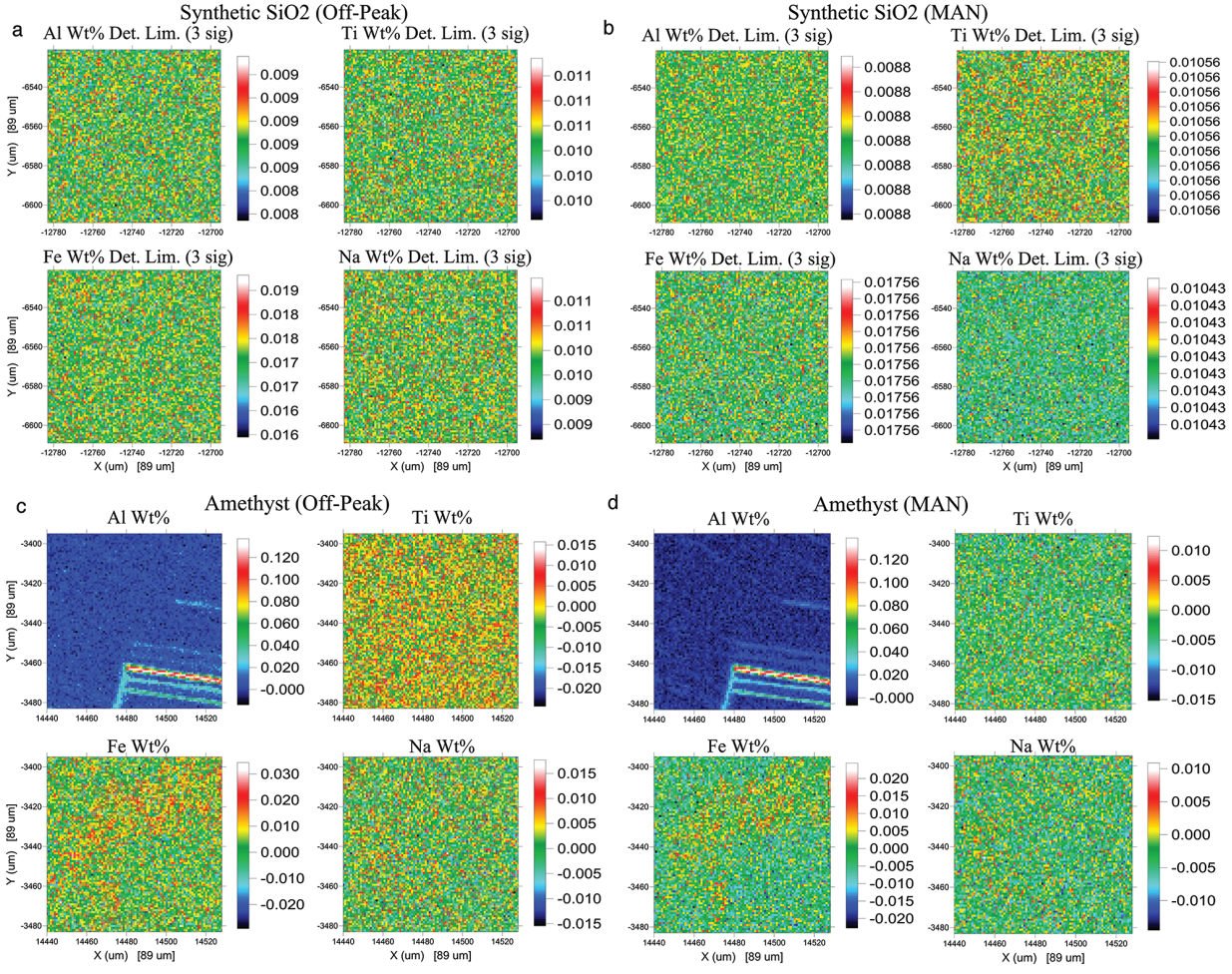

Figure 9. (**a**) Calculated detection limits in synthetic SiO_2, 15 keV, 100 nA, 6000 ms, 3000 ms off-peak (×2) with off-peak processing and no blank correction. Off-peak sensitivity is a combination of both the on-peak and off-peak counting statistics. (**b**) Calculated detection limits in synthetic SiO_2, 15 keV, 100 nA, 6000 ms on-peak only, MAN background correction and no blank correction. Because the MAN background method is dominated essentially by the on-peak counting statistics, we obtain better sensitivity in approximately half the counting time. (**c**) Al, Ti, Fe, and Na wt% in Reed amethyst (Butte, Montana), 15 keV, 100 nA, 6000 ms on-peak, and 3000 ms off-peak (×2) using off-peak background corrections and blank corrected. (**d**) Al, Ti, Fe, and Na wt% in Reed amethyst (Butte, Montana), 15 keV, 100 nA, 6000 ms on-peak using MAN (on-peak) intensities only and blank corrected.

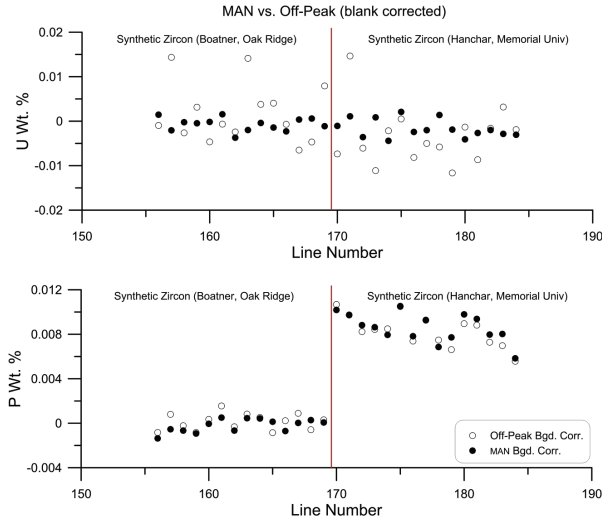

FIGURE 10. Point analyses on two synthetic zircons for both off-peak measured and MAN calculated background intensities for U and P. Acquisition conditions were 20 keV, 100 nA, 10 μm, 200 s on-peak (200 s off-peak). Note the somewhat larger variance in the off-peak data for U and what appears to be ~80 ppm of P in the Hanchar zircon compared to the Oak Ridge zircon.

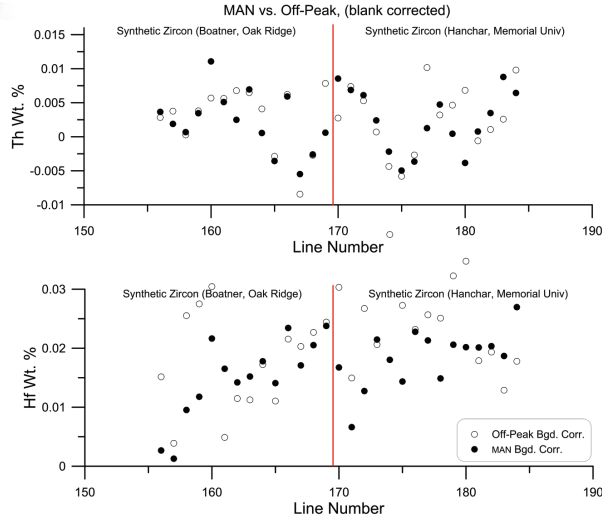

Figure 11. Point analyses (line profile with approximately 30 μm spacing) on two synthetic zircons for both off-peak measured and MAN calculated background intensities for Th and Hf. Acquisition conditions were 20 keV, 100 nA, 10 μm, 200 s on-peak (100 s off-peak, ×2). Although the concentrations and variances for these elements are similar for both background correction methods, use of the MAN background correction requires half the acquisition time of the traditional off-peak method.

oxygen isotope standard AS3) for U, Th, Y, P, and Hf. Figures 10 and 11 shows results for blank-corrected point analyses of two synthetic zircons, the first grown by John Hanchar at Memorial University and the second, grown by Lynn Boatner at Oak Ridge National Laboratory for U, P, Hf, and Th. The only observable statistical result was for P at approximately 80 ppm higher in the Hanchar material than the Oak Ridge Laboratory material.

Figures 12a and 12b compare the calculated background intensities for X-ray maps (based three X-ray map acquisitions for each sample: the on-peak intensity pixel map, the high side pixel intensity map and the low side pixel intensity map—note that MAN results utilize only the on-peak intensity map), calculated for four of these elements after applying both the off-peak and MAN background correction methods using the same raw intensity acquisition data set on the zircon sample for both background correction methods for the quantitative results in Figures 12c and 12d. Again we can see that the variance of the off-peak measured and interpolated background intensities are significantly larger than the same data calculated using the MAN method (using only the measured on-peak intensities and the MAN calibration curve standards of synthetic $MgSiO_4$, $FeSiO_4$, $MnSiO_4$, $CoSiO_4$, $NiSiO_4$, $PbSiO_4$, and $ThSiO_4$). Finally, Figures 13a and 13b compare detection sensitivity for both background correction methods.

Background intensity and elemental concentration maps are shown in Figure 14 for the natural zircon SIMS oxygen standard where some trace heterogeneity can be seen in the Hf map. The improvement in precision for the MAN method (and the maintaining of accuracy) is easily seen in the last figure (Fig. 15), where the U concentration profile across the concentration maps in Figures 14c and 14d are shown for both the off-peak and MAN methods calculated from the same acquisition data set.

Accuracy vs. precision in the MAN background method

When we consider traditional off-peak measurements we obtain a variance from the on-peak measurement and a variance from the off-peak measurement. When these measured on-peak and high and low off-peak intensities are subtracted from each other, the errors add in quadrature as described above. In the case of Nth point off-peak measurements, the variances are solely due to the on-peak variances and the off-peak intensity is a constant. As is the case with traditional and Nth point off-peak methods, the MAN background method variance is also dominated by the on-peak statistics, but with a minor contribution from the major element statistics and the slope of the MAN regression, rather than the Gaussian statistics of the continuum. In the case where these major elements are measured, the MAN variance depends on the major element counting statistics and in the case where these major elements are simply specified as fixed concentrations or by difference, only the trace element variances contribute toward the determination of average atomic number variance.

Some analysts have pointed out that there must be a precision or error associated with the MAN regression as derived for Model A, yet we do not observe this correlation variance in replicate measurements. We can see this by comparing actual measured background intensity variances from off-peak measurements with a fixed matrix, MAN measurements with a fixed matrix and MAN measurements with measured matrix elements) with the calculated sensitivities for the off-peak and MAN methods, respectively, from our MAN variance model as seen in Table 3. In Table 3a, we compare the average and standard deviation for the calculated off-peak background intensities from off-peak (analogous to Fig. 12a), that is, measured

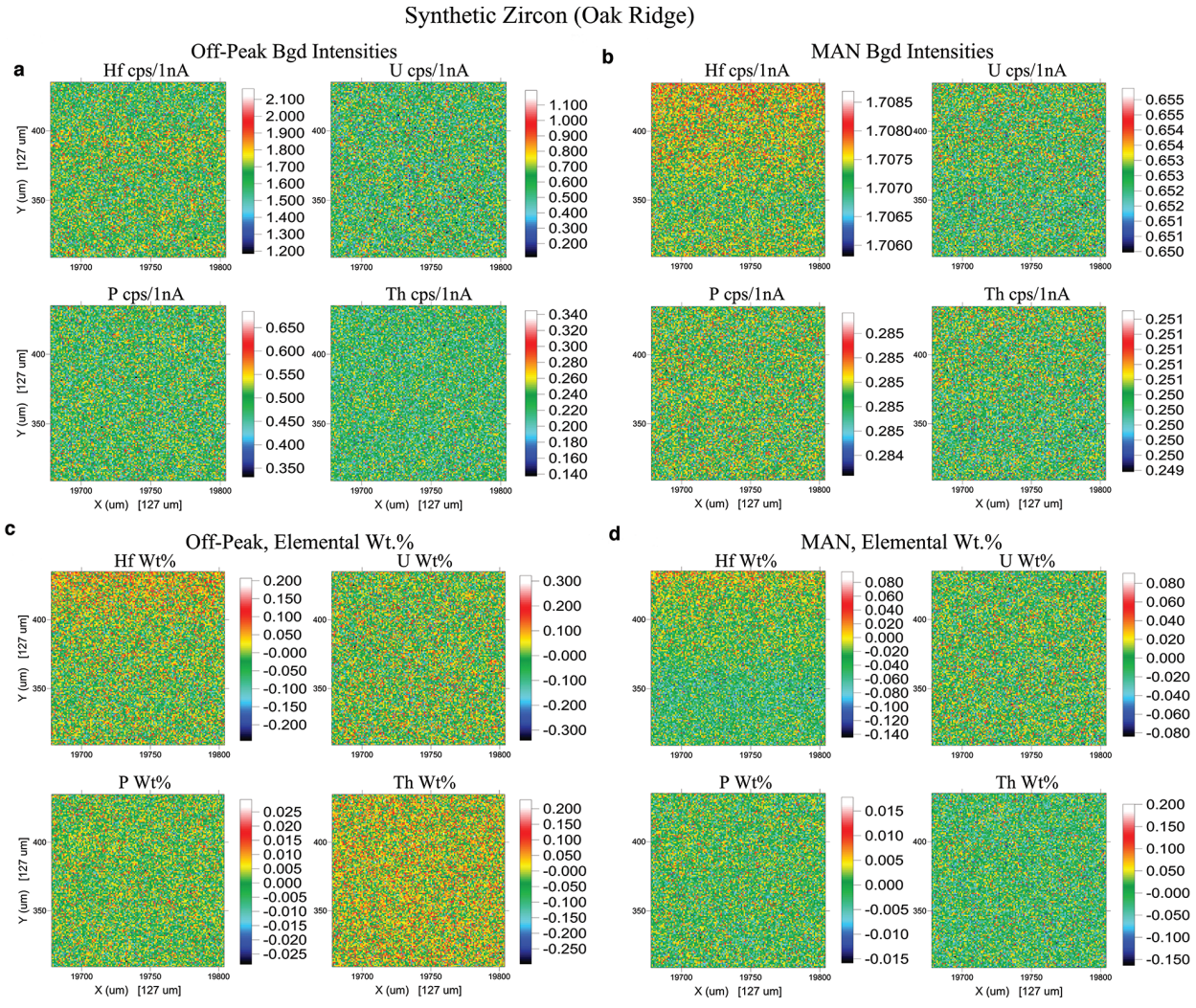

Figure 12. (**a**) Calculated background intensities in a synthetic zircon (no. 257 from Lynn Boatner at Oak Ridge) using a linear interpolation of the measured off-peak pixel intensities using high side and low side off-peak positions for Hf*M*α, U*M*α, P*K*α, and Th*M*α. Conditions were 20 keV, 100 nA, 3000 ms on-peak, 1500 ms off-peak (×2). Note that the calculated background intensities show the expected variance from the off-peak measurement uncertainties. (**b**) Calculated background intensities using a linear regression curve from the measured on-peak intensities for several standard materials that do not contain the elements of interest. Hf*M*α, U*M*α, P*K*α, and Th*M*α, at 20 keV, 100 nA, 3000 ms on-peak only. Note that the calculated MAN background intensities show a much smaller degree of variance than the off-peak background intensities in **a**. Also note that the calculated off-peak backgrounds in **a** for P*K*α are much higher than the MAN calculated background intensities in this figure. This difference is due to significant interference from Zr *L* lines family on the P*K*α (low side) off-peak position. In other words, because MAN backgrounds do not utilize any off-peak data, there is no off-peak interferences for the MAN background method and hence a more accurate background correction in this case. Finally note the slightly greater concentration of Hf in the upper part of the map causes a slightly higher average *Z* to be calculated (and hence a slightly higher MAN background intensity to be derived from the MAN calibration curve), which is only visible in the MAN background map. (**c**) Calculated elemental concentrations in a synthetic zircon using a linear interpolation from the measured off-peak intensities for Hf*M*α, U*M*α, P*K*α, and Th*M*α. Conditions were 20 keV, 100 nA, 3000 ms on-peak, and 1500 ms off-peak (×2) and blank corrected. Note that the calculated concentrations from the off-peak measurements show larger variations than the MAN background corrected intensities due to the variance of the off-peak measurements in **a**. (**d**) Calculated elemental concentrations in a synthetic zircon using MAN calibration curves corrected for continuum absorption for Hf*M*α, U*M*α, P*K*α, and Th*M*α. Conditions were 20 keV, 100 nA, 3000 ms on-peak only and blank corrected. Note the variation in the Hf concentration map is significantly smaller for the MAN corrected map than the off-peak corrected map in **c** due to the greater precision of the MAN method.

and interpolated under the peak, with the calculated background variance by assuming Gaussian statistics on the peak and background and adding them in quadrature as discussed previously. As one can see, the calculated and modeled off-peak intensity variances are quite similar.

For comparison with MAN background intensity statistics, we can examine Table 3b, which shows the average and standard deviation of the measured and regressed MAN background

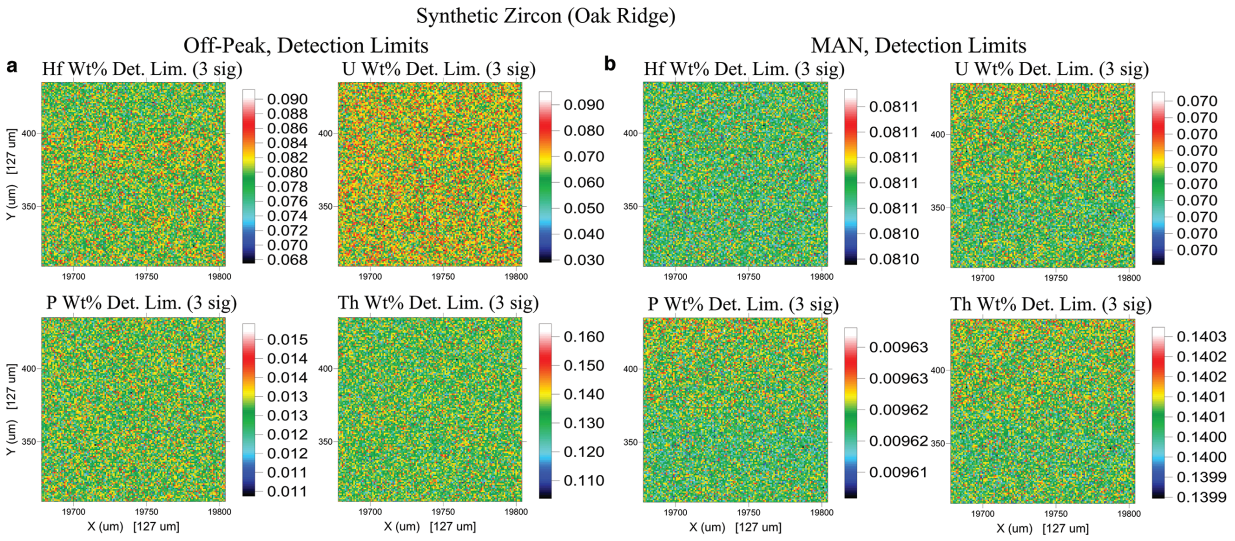

Figure 13. (**a**) Calculated detection limits in synthetic zircon (Boatner), 15 keV, 100 nA, 3000 ms, 1500 ms off-peak (×2) off-peak background correction without the blank correction. Off-peak sensitivity is a combination of on-peak and off-peak counting statistics. (**b**) Calculated detection limits in synthetic zircon (Boatner), 15 keV, 100 nA, 3000 ms on-peak only, MAN background correction and without a blank correction. The detection limit calculation in the case of the MAN background method is essentially dominated by only the on-peak counting statistics since the matrix elements are fixed by specification.

intensities obtained by calculation of the average Z and MAN regression curve when the matrix major elements are fixed (analogous to Fig. 12b), with the modeled MAN sensitivities from our MAN sensitivity/variance expressions, for both model A (using the full MAN variance expression including the terms for the MAN regression precision) and model B (using the modified MAN variance expression without the MAN regression precision terms). As can be seen, by including the MAN regression precision terms in the MAN variance model (model A), we obtain variances that are approximately 100 times greater than the variances of the calculated MAN background intensities from our quantification procedures. On the other hand, using model B, we obtain predicted MAN background variances that agree quite well with MAN background measurements. The reason the MAN variances are so small in Table 3b compared to the off-peak background variances in Table 3a, is that the matrix elements (Zr, Si, and O) were specified as a fixed concentration (statistically similar to the Nth point constant background method). This can easily be seen in the elemental concentration data for U in Figure 15 where the off-peak and MAN calculated concentrations are compared. In this case of fixed matrix elements, the only contribution to the average Z variance is from the measured trace elements. As expected, specifying the matrix as $ZrSiO_4$ by difference from 100% (not shown) yields almost exactly the same measured MAN intensities and variances as using a fixed compositional matrix.

In Table 3c, we again compare the measured and calculated variances, but this time with Zr and Si measured analytically and oxygen calculated by stoichiometry. In this case where the major elements are measured, the actual MAN background variance is slightly larger than with the fixed or by difference compositional matrix as seen in Table 3b. But again, model A produces predicted MAN background variances that are approximately 10 times greater than we observe in the calculated MAN background intensities, while using model B the measured and calculated MAN background intensity variances are again very similar, thus demonstrating the validity of our MAN sensitivity model without including the MAN regression precision terms, as unintuitive as this may seem.

Another way to consider the issue of accuracy and precision in the MAN method is to realize that if one re-measures intensities utilized for the MAN regression curve, the fit coefficients will be slightly different, giving a slightly different background intensity for the same average Z, when compared to the previous MAN calibration. However, this intensity difference between subsequent MAN regressions merely represents a systematic accuracy error, since each single new MAN regression fit will repeatedly produce the same high-precision intensity for a given composition (and hence average Z) for every new unknown measurement, resulting in improved precision when it is subtracted from the on-peak measurement. Indeed, if we did re-measure the MAN calibration curve intensities for every point analysis and every X-ray map pixel, then we would need to include the MAN regression precision in our sensitivity calculations. But in fact, we do not re-measure the MAN intensities for every unknown measurement and instead correct for MAN accuracy using the blank correction.

A principal challenge for users of the MAN background method is limiting the unknown $\overline{Z}$ variance through high-precision analysis of major elements or by restriction to simple matrices (with fixed concentration or by difference major elements). Maximizing the accuracy of the MAN regression depends on primary standards that are pure, homogeneous, and do not contain the element of interest and proper correction of continuum absorption. In practice, a few simple metals or

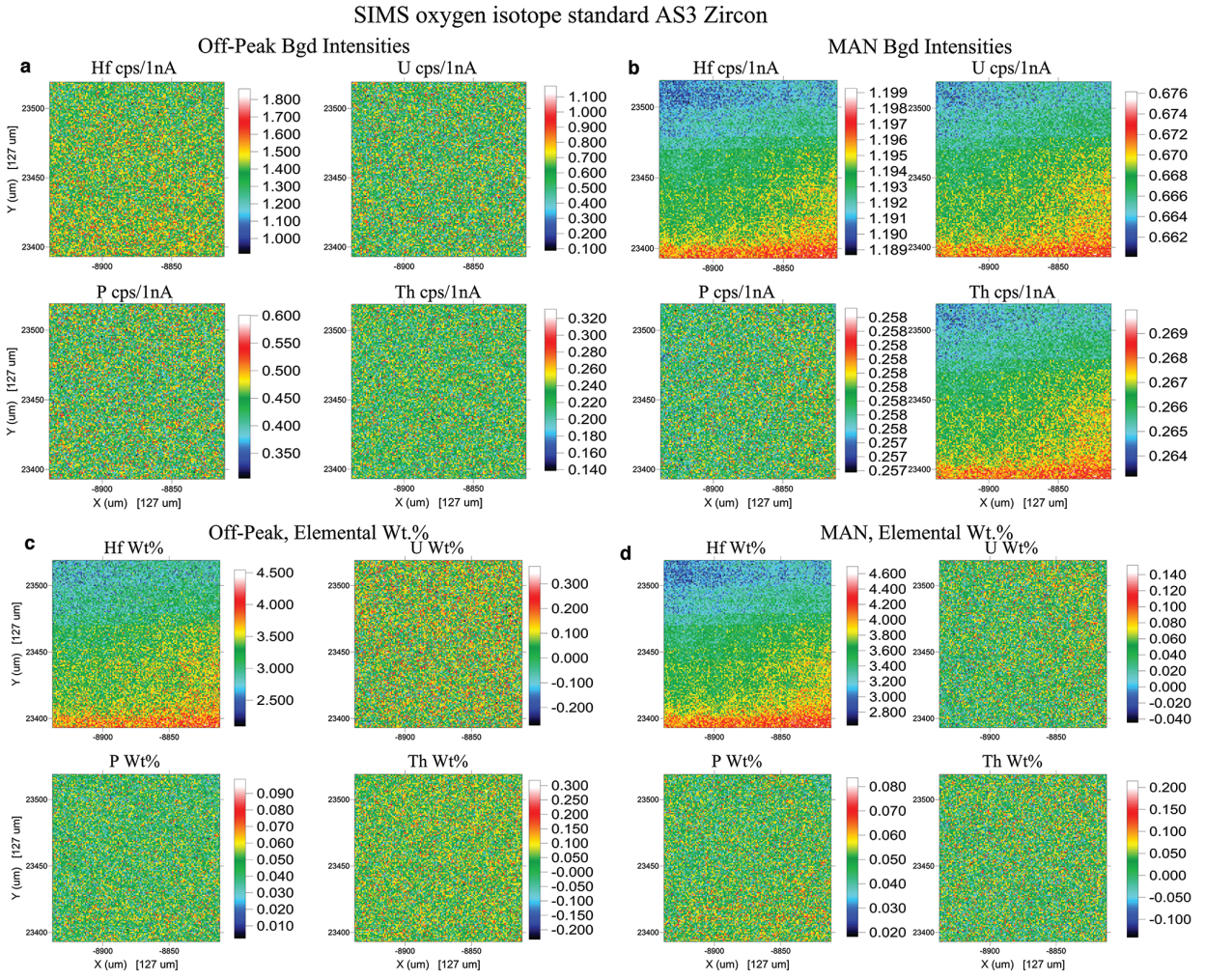

Figure 14. (**a**) Calculated background intensities in SIMS oxygen isotope standard AS3 zircon using a linear interpolation from the measured off-peak intensities for Hf*Mα*, U*Mα*, P*Kα*, and Th*Mα*. Conditions were 20 keV, 100 nA, 4000 ms on-peak, 2000 ms off-peak (×2). (**b**) Calculated background intensities in SIMS oxygen isotope standard AS3 zircon using MAN calibration curves corrected for continuum absorption for Hf*Mα*, U*Mα*, P*Kα*, and Th*Mα*. Conditions were 20 keV, 100 nA, 4000 ms on-peak only. Note that the calculated MAN background intensities show a much smaller degree of variance than the off-peak background intensities in **a**. (**c**) Calculated elemental concentrations in a natural SIMS oxygen isotope standard AS3 zircon using a linear interpolation from the measured off-peak intensities for Hf*Mα*, U*Mα*, P*Kα*, and Th*Mα*. Conditions were 20 keV, 100 nA, 4000 ms on-peak, 2000 ms off-peak (×2). Note that the calculated concentrations for U and Th from these off-peak corrected measurements are consistently lower compared to the MAN background corrected concentrations as seen in **d**, due to subtle interferences and continuum artifacts in the off-peak measurements. (**d**) Calculated elemental concentrations in a natural SIMS oxygen isotope standard AS3 zircon using MAN calibration curves corrected for continuum absorption for Hf*Mα*, U*Mα*, P*Kα*, and Th*Mα*. Conditions were 20 keV, 100 nA, and 4000 ms on-peak only.

oxides such as MgO, Al_2O_3, SiO_2, TiO_2, MnO, and NiO will suffice for calibrating the continuum for various emission lines in most silicates and oxides. If such standards are used, then the correlation variances will be inherently minimized and accuracy improved by avoiding MAN standards that interfere with the on-peak measurement positions.

Calculation of detection limits with the MAN background method

Because the MAN background intensity variation does not follow Gaussian statistics, we cannot base our sensitivity concentration of detection limit (CDL) calculations on traditional expressions, which only utilize the background variance. Instead, we must add our calculated MAN background variance to our on-peak variance as previously described to obtain a net concentration variance. There are several methods traditionally utilized to calculate the minimum detection limit (CDL) for off-peak intensity measurements. One method is to assume that three times the variance of the raw photon intensity, expressed as a concentration and corrected for matrix effects, yields a 99% confidence estimate of detection limits (Scott et al. 1995) as seen here:

TABLE 3a. Comparison of off-peak background measurement and interpolation for all background intensity map pixels (analogous to Fig. 17) with calculated off-peak variance (average of all pixels) assuming Gaussian statistics (square root of raw photon intensity)

	Th	Hf	U	P	Y
Average	0.226061	2.02225	0.611455	0.320043	0.113804
St.dev.	0.028376	0.142604	0.128880	0.037488	0.021821
Off-peak model	0.027325	0.081837	0.044766	0.032520	0.019335

Notes: All values in cps/nA. The variation from the measured off-peak intensities and the calculated variance model is excellent except for Hf and U, where the measured variation is somewhat larger. This larger variation for Hf and U could be due to trace concentration variation in the standard material.

TABLE 3b. Comparison of MAN background calculations for all background intensity map pixels with fixed matrix (analogous to Fig. 18) (Zr 49.764, Si 15.322, O 34.914 wt%) with the calculated MAN background variance (average of all pixels) from our model

	Th	Hf	U	P	Y
Average	0.254557	2.04241	0.630875	0.280978	0.113875
St.dev.	0.000348	0.001509	0.002499	0.000904	0.000156
MAN model (A)	0.025887	0.076575	0.026831	0.017200	0.006861
MAN model (B)	0.000328	0.001510	0.000612	0.000265	0.000095

Notes: Model A is using the full MAN variance expression with the terms for the MAN regression precision, and model B is the modified MAN variance expression without the MAN regression precision terms. Note that since the $ZrSiO_4$ matrix is specified and therefore constant, the average atomic number variance is minimal for the MAN regression curve. However, model A, which includes the MAN regression precision terms of the MAN variance expression, results in predicted background intensity variances that are approximately 100 times larger than observed in the actual data, while model B, without the MAN regression precision terms, produces predicted variances that are in excellent agreement with the actual MAN background intensity variances.

TABLE 3c. Comparison of MAN background calculations for all background intensity map pixels with a measured $ZrSiO_4$ matrix

	Th	Hf	U	P	Y
Average	0.254586	2.04253	0.630940	0.281020	0.113894
St.dev.	0.000812	0.002682	0.002897	0.001754	0.000683
MAN Model (A)	0.027446	0.083754	0.029741	0.018462	0.007315
MAN Model (B)	0.001886	0.008685	0.003521	0.001526	0.000549

Notes: Again model A is using the full MAN variance expression with the terms for the MAN regression precision, and model B is the modified MAN variance expression without the MAN regression precision terms. Since the major elements are actually measured here (relative to a $ZrSiO_4$ standard), the average atomic number variance is dominated by the major element concentration variation. Therefore the measured and predicted (modeled) variances are somewhat larger than the fixed matrix variances seen in Table 3b as expected. However, model A, which includes the MAN regression precision terms of the MAN variance expression, results in predicted background intensity variances that are approximately 10 times larger than observed in the actual data, while model B, without the MAN regression precision terms, produces predicted variances that are in excellent agreement with the actual MAN background intensity variances.

$$C_{CDL} = \frac{3\sqrt{I_B}}{I_S}.$$

However, because the variances of the calculated MAN background intensities do not follow Gaussian statistics, we cannot simply assume this for the MAN detection limit. In the limit as the background variance approaches zero, this definition of the CDL approaches zero (infinitely low). Instead we will need to utilize the net intensity variance for the MAN sensitivity calculation. Based on the off-peak net intensity variance expression we will propose that the MAN net intensity variance is similarly expressed as:

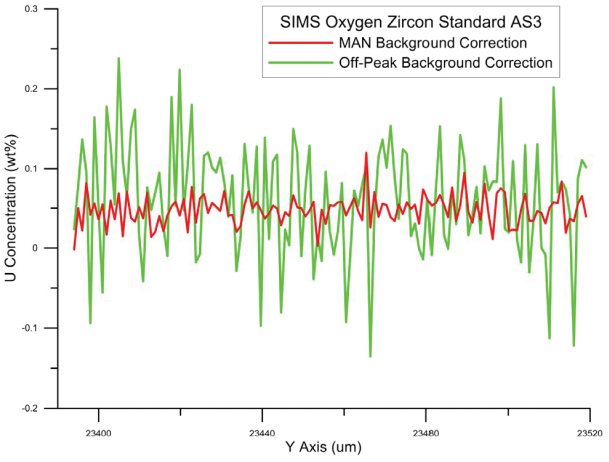

FIGURE 15. Line profiles for both off-peak and MAN background methods for the U concentration maps in Figures 14c and 14d. Here we can easily see that accuracy is maintained and precision is significantly improved, while in practice, the MAN method acquisition would take half the acquisition time of the off-peak trace element maps.

TABLE 4. Comparison of measured variances in replicate measurements of Oak Ridge zircon at 20 keV, 100 nA, average of 5 points for off-peak and MAN measurements, with and without the blank correction

	Th wt%	Hf wt%	U wt%	P wt%	Y wt%
Off-peak, No blank					
Average	0.002138	0.01171	0.013602	–0.00505	–0.00947
St.dev.	0.006832	0.005244	0.005994	0.000706	0.005989
Off-peak, Blank					
Average	0	0.001499	0.000001	0.000001	0.002501
St.dev.	0.006832	0.005243	0.005994	0.000706	0.005989
Nth Point, No blank					
Average	0.001715	0.007501	0.018374	–0.00611	–0.00796
St.dev.	0.004528	0.003775	0.001211	0.000376	0.002593
Nth Point, Blank					
Average	0	0.001499	0.000002	0.000001	0.002501
St.dev.	0.004529	0.003775	0.001211	0.000376	0.002593
MAN, No blank					
Average	–0.05026	0.014599	–0.04495	0.028541	0.025386
St.dev.	0.00447	0.00417	0.001219	0.000387	0.002595
MAN, Blank					
Average	–0.00092	0.001398	–0.00071	–0.00005	0.00222
St.dev.	0.004469	0.004169	0.001219	0.000387	0.002595

Notes: As expected the measured variances (St.dev.) are almost identical between the blank and non-blank measurements. Note also that the Nth Point and MAN background methods give similar standard deviation results in about the same acquisition time, the difference being that the Nth Point background method cannot handle compositional heterogeneity, while the MAN background method can.

$$\sigma_{MAN_{net}} = \sqrt{\sigma_P^2 + \sigma_B^2}$$

where in this case, σ_P is the calculated MAN intensity under the peak, and σ_B is the calculated MAN background variance from the model B MAN variance expression. In the case of a fixed composition matrix, e.g., $ZrSiO_4$ by difference (see Table 3b), the value of σ_B approaches zero, so we can compare the situation where we have a normal peak variance and

a zero background variance (as we would in the case of Nth point off-peaks), and find that as σ_B approaches zero our net intensity statistics are improved by a factor of square root of 2 or roughly a third as the MAN background variance approaches zero. Therefore, at least in the case of our fixed composition matrix, we should expect to obtain MAN detection limits that are roughly a third better than traditional off-peak measurements.

Comparing off-peak detection limits calculated by assuming three times the background variance, we find that using two net intensity variances we obtain a MAN CDL that is approximately a third better, which is not surprising since the MAN background variance term is close to zero. Figures 9a and 9b for SiO_2 and Figures 13a and 13b for $ZrSiO_4$ demonstrate this.

Finally see Table 4 for a comparison of blank and non-blank corrected measurement results for the Oak Ridge synthetic zircon for off-peak, Nth Point, and MAN background methods, where it can be seen that the application of the blank correction results in an insignificant increase in the absolute standard deviation, which is due to the fact that the blank correction itself is small compared to the total background, and the blank standard calibration (as is the case with the MAN standard intensities), is measured only once, but then applied repeatedly to subsequent replicate data sets to improve accuracy. Again, if we did re-measure the blank correction for every point acquisition or X-ray map pixel, we would indeed need to include the blank correction variance in the trace element sensitivity for all background methods. But since we do not generally re-measure the blank standard for every point or pixel acquisition, we are merely limiting our blank accuracy to the precision of the blank standard measurement.

Acknowledgments

We thank our informal reviewers Paul Carpenter at Washington University and Michel Jercinovic at the University of Massachusetts at Amherst for valuable suggestions and critical comments and feedback. We also acknowledge funding from NSF EAR-0345908 and the Murdoch Foundation for purchase of the Cameca SX100 EPMA instrument. We additionally acknowledge the gracious donation of synthetic zircons from Lynn Boatner at Oak Ridge National Laboratory and John Hanchar at Memorial University. The synthetic quartz and zircon were characterized for trace elements by Allan Koenig at the USGS in Denver, Colorado. The natural zircon SIMS standard was provided by Dylan Colon and Ilya Bindeman at the University of Oregon. The authors would also like to thank two anonymous reviewers for their helpful suggestions and comments.

References cited

Armstrong, J.T. (1988) Quantitative analysis of silicate and oxide materials: Comparison of Monte Carlo, ZAF, and procedures. Microbeam Analysis, 239–246.

Donovan, J.J., and Pingitore, N. (2002) Compositional averaging of continuum intensities in multielement compounds. Microbeam Analysis, 8, 429–436.

Donovan, J.J., and Tingle, T. (1996) An improved mean atomic number background correction for quantitative microanalysis. Journal of Microscopy and Microanalysis, 2, 1–7, http://www.probesoftware.com.

Donovan, J.J., Snyder, D.A., and Rivers, M.L. (1993) An improved interference correction for trace element analysis. Microbeam Analysis, 2, 23–28.

Donovan, J.J., Lowers, H.A., and Rusk, B.G. (2011) Improved electron probe microanalysis of trace elements in quartz. American Mineralogist, 96, 274–282.

Kato, T., and Suzuki, K. (2014) "Background holes" in X-ray spectrometry using pentaerythritol (PET) analyzing crystal. Journal of Mineralogical and Petrological Sciences, 109, 151–155.

Kramers, H. (1923) On the theory of X-ray absorption and the continuous X-ray spectrum. Philosophical Magazine, 46, 836.

Scott, V.D., Love, G., and Reed, S.J.B. (1995) Quantitative Electron-Probe Microanalysis, 2nd ed., 105 p. Ellis Horwood Series Physics and its Applications.

Ware, N.G., and Reed, S.J.B. (1973) Background corrections for quantitative electron microprobe analysis using a lithium drifted silicon X-ray detector. Journal of Physics E: Scientific Instruments, 6, 286–288.

Manuscript received November 18, 2015
Manuscript accepted March 24, 2016
Manuscript handled by Adam Kent